Vortex-antivortex configurations and its stability in a mesoscopic superconducting square

T. Mertelj[1,2] and V. V. Kabanov[1]
[1]*J. Stefan Institute, Jamova 39, 1000 Ljubljana, Slovenia*
[2]*Faculty of Mathematics and Physics, Jadranska 19, University of Ljubljana, Ljubljana, Slovenia*
(Received 28 November 2002; revised manuscript received 7 February 2003; published 30 April 2003)

We solve the Ginzburg-Landau equation for the mesoscopic superconducting thin film of square shape in a magnetic field for a wide range of Ginzburg-Landau parameters $0.05<\kappa_{eff}<\infty$. We focus on the region of the field where the formation of an antivortex has been reported previously. We found that the phase with the antivortex exists in the broad range of parameters. When the coherence length decreases the topological phase transition to the phase with the same total vorticity and a reduced symmetry takes place. The giant vortex with vorticity $m=3$ is found to be unstable for any field, ξ/a and $\kappa_{eff}\gtrsim 0.1$. Reduction of κ_{eff} does not make the phase with antivortex more stable contrary to the case of a cylindric sample of the type-I superconductor.

DOI: 10.1103/PhysRevB.67.134527 PACS number(s): 74.25.Op, 74.25.Ha, 74.81.−g

I. INTRODUCTION

Recently it was shown that the influence of boundaries can lead to stabilization of the vortex-antivortex molecules in mesoscopic samples.[1] Analysis of the linearized Ginzburg-Landau equation (GLE) has shown that such molecules appear at particular values of the external magnetic field depending on the sample shape and size.[2] The solution of the GLE in the limit of the extreme type-II superconductor shows that such molecules have a very shallow minimum in the free energy[3,4] and are very sensitive to the change of the sample shape.[5]

In a square mesoscopic thin film with the total vorticity $m=3$ the symmetric solution with four vortices and one antivortex is the solution of the linearized GLE with the lowest free energy.[1] According to Ref. 3, away from the H_{c2} line the giant vortex with vorticity $m=3$ is stable and has the lowest free energy. This implies that a topological phase transition *without change* of the vorticity and *without a reduction* of the symmetry should take place with the change of the external field and/or the coherence length away from the critical-field line.

It was proposed that in the limit $\kappa\simeq 1/\sqrt{2}$, where the vortex-antivortex interaction changes sign, vortex-antivortex complexes should be more stable[6] for the cylindric sample shape. For a thin film with $\lambda_{eff}=\lambda^2/d$ and $\kappa_{eff}=\lambda_{eff}/\xi$, where d is the thickness of the film, λ is the London penetration depth, and ξ is the superconducting coherence length, this mechanism should be less effective due to a smaller contribution of the ''magnetic energy'' to the total free energy.

We performed an extensive study of the region of the phase diagram where the vortex-antivortex phase was previously reported for a sample of square shape.[1] We focused on the region $4<a/\xi<8$ and $\kappa_{eff}>0.05$. We found that the antivortex phase is stable in a broad range of parameters. The region of stability of the phase does not depend strongly on the value of the parameter κ_{eff}. The energy gain due to the antivortex formation is much smaller then the energy difference between two phases with different vorticities. The giant vortex with $m=3$ is unstable for any field, ξ/a and $\kappa_{eff}\gtrsim 0.1$. The phase transition to the phase with three separated vortices takes place when ξ/a is driven away from the critical-field line. The reduction of κ_{eff} does not stabilize the antivortex phase for the thin film sample in the contrast to the case of the cylindric sample.[6]

II. FORMALISM AND SOLUTION

The GLE for the normalized complex order parameter $\psi=\Psi/\Psi_0$, $\Psi_0=\sqrt{\beta/|\alpha|}$, has the following form:

$$\xi^2\left(i\nabla+\frac{2\pi\mathbf{A}}{\Phi_0}\right)^2\psi-\psi+\psi|\psi|^2=0; \tag{1}$$

here $\xi=\hbar^2/4m|\alpha|$, α and β are the temperature-dependent parameters of the Ginzburg-Landau expansion for the free energy, Φ_0 is the flux quantum, $\mathbf{A}$ is the vector potential, and $\mathbf{H}=\nabla\times\mathbf{A}$ is the magnetic field. The second GLE equation for the vector potential reads

$$\nabla\times\nabla\times\mathbf{A}=-i\frac{\Phi_0}{4\pi\lambda^2}(\psi^*\nabla\psi-\psi\nabla\psi^*)-\frac{|\psi|^2\mathbf{A}}{\lambda^2}. \tag{2}$$

In addition to Eq. (1) we assume the boundary condition for the superconductor-insulator junction on the sample edges:

$$\left(i\nabla+\frac{2\pi\mathbf{A}}{\Phi_0}\right)\cdot\mathbf{n}\psi=0, \tag{3}$$

where $\mathbf{n}$ is a vector normal to the surface of the sample.

As was described in Ref. 3 we introduce $N\times N$ discrete points on the square and rewrite Eq. (1) in the form of the nonlinear discrete Schrödinger equation

$$\sum_{\mathbf{l}} t_{\mathbf{i}+\mathbf{l},\mathbf{i}}\psi_{\mathbf{i}+\mathbf{l}}-\epsilon(\mathbf{i})t_{\mathbf{i},\mathbf{i}}\psi_{\mathbf{i}}-\psi_{\mathbf{i}}+\psi_{\mathbf{i}}|\psi_{\mathbf{i}}|^2=0, \tag{4}$$

where the summation index $\mathbf{l}=(\pm1,0),(0,\pm1)$ points toward the nearest neighbors and $t_{\mathbf{i}_1,\mathbf{i}}=(\xi N/a)^2\exp(i\phi_{\mathbf{i}_1,\mathbf{i}})$ and $\phi_{\mathbf{i}_1,\mathbf{i}}=-(2\pi/\Phi_0)\int_{\mathbf{r}_\mathbf{i}}^{\mathbf{r}_{\mathbf{i}_1}}\mathbf{A}(\mathbf{r})d\mathbf{r}$. The boundary conditions are included in the discrete nonlinear Schrödinger equation as in

Ref. 3 where $\psi_{\mathbf{i}}=0$ if $\mathbf{i}$ is outside of the sample and $\epsilon(\mathbf{i})=4-\delta_{i_x,1}-\delta_{i_x,N}-\delta_{i_y,1}-\delta_{i_y,N}$ where $\mathbf{i}=(i_x=1,\ldots,N,i_y=1,\ldots,N)$.

After discretization of Eq. (2) we can obtain the exact expression for the vector potential:

$$A^v_{\mathbf{i}}=\sum_{\mathbf{n}} K(\mathbf{i}-\mathbf{n})J^v_{\mathbf{n}}, \tag{5}$$

where

$$J^v_{\mathbf{i}}=\frac{\Phi_0 a}{4\pi\lambda_{eff}N}\mathrm{Im}[\exp(-i\phi_{\mathbf{i}+\mathbf{l}_v,\mathbf{i}})\psi^*_{\mathbf{i}}\psi_{\mathbf{i}+\mathbf{l}_v} - \exp(-i\phi_{\mathbf{i}-\mathbf{l}_v,i})\psi^*_{\mathbf{i}}\psi_{\mathbf{i}-\mathbf{l}_v}], \tag{6}$$

where $v\in\{x,y\}$ and $\mathbf{l_x}=(1,0)$, $\mathbf{l_y}=(0,1)$, and

$$K(\mathbf{n})=\frac{N}{2\pi^2 a}\int_0^\pi dxdy\frac{\cos(n_x x)\cos(n_y y)}{\sqrt{4-2\cos(x)-2\cos(y)}}. \tag{7}$$

The numerical self-consistent solution of the problem is obtained by iterating the solution of the nonlinear equation for the order parameter, Eq. (4), and calculations of the current and the vector potential, Eqs. (5) and (6). We used two ways of solving Eq. (4). The first is similar to that reported in Ref. 3 and corresponds to the iterative solution of the linearized equation (4). The second relies on the fact that Eq. (4) represents the Euler equation for the free-energy functional with included boundary conditions. Equation (4) was therefore solved by the direct minimization of the corresponding functional using the conjugate-gradient method. Both techniques gave identical results.

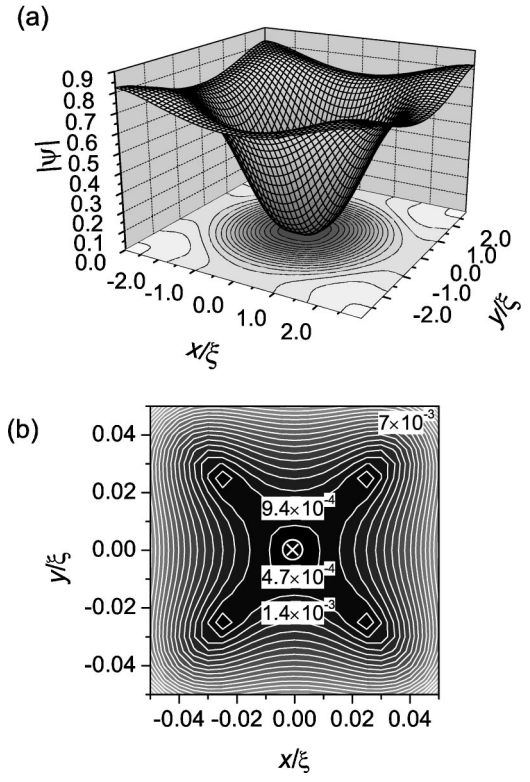

FIG. 1. (a) The magnitude of the superconductivity order parameter for $(a/\xi)^2=35$, $\kappa_{eff}=\infty$, and $\Phi=5.9\Phi_0$. (b) The central region where the vortices are located in an expanded scale. The position of the antivortex is indicated by the symbol $\otimes$.

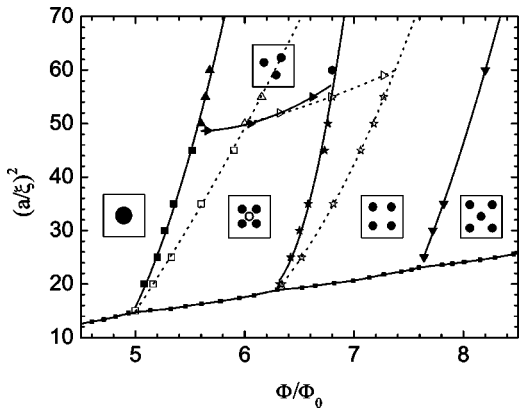

FIG. 2. The calculated phase diagram. Different phases are marked with icons schematically indicating the vortex pattern where the solid circle represents a vortex, the open circle represents an antivortex, and the larger solid circle represents a double vortex. The solid symbols and solid lines represent the phase boundaries for $\kappa_{eff}=\infty$ while the open symbols and dotted lines represent the phase boundaries for $\kappa_{eff}=1$. In the latter case only the phase boundaries of the region with the total vorticity 3 are shown.

III. RESULTS

The main goal of the paper is to investigate the phase diagram in the region $4.5<\Phi/\Phi_0<6.5$ and $(a/\xi)^2<60$ where the solution with one antivortex and four vortices (Fig. 1) has been reported. We found that the region of the phase diagram where the symmetry-induced antivortex solution has the lowest energy is broader than expected from the solution of the linearized GLE. As is shown in Fig. 2 for $\kappa_{eff}=\infty$ the antivortex phase is stable up to $(a/\xi)^2\sim 55$, depending on Φ/Φ_0. For a finite κ_{eff} this region shifts to the higher field as $(a/\xi)^2$ increases (see Fig. 2).

The interesting behavior is observed when the external

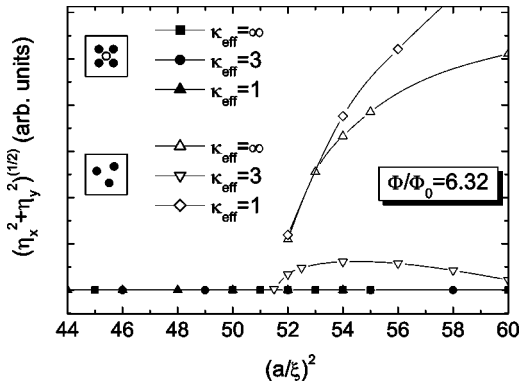

FIG. 3. The magnitude of the order parameter around the transition where one vortex annihilates with the antivortex as a function of $(a/\xi)^2$ at constant magnetic field.

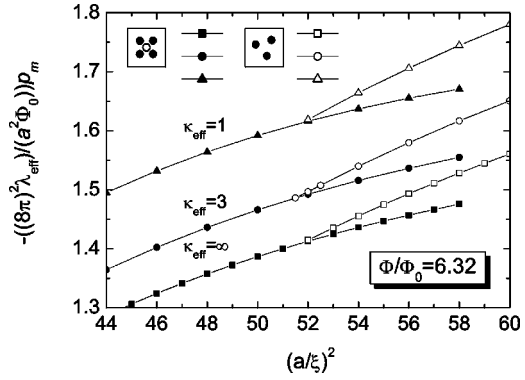

FIG. 4. The magnetic moment of the sample as a function of $(a/\xi)^2$ at constant magnetic field.

field is fixed and $(a/\xi)^2$ increases. Close to the H_{c2} the lowest minimum of the free energy corresponds to the solution with the vorticity $m=4-1$ with the antivortex in the center of the square. Present calculations do not confirm the existence of the giant-vortex solution with $m=3$ in this region of the phase diagram as reported previously.[3] The difference is due to the increase of the number of discrete points N enabling detection of the antivortex. With increase of $(a/\xi)^2$ away from the H_{c2} line the phase transition to the multivortex state with the same vorticity $(m=3)$ and a lower symmetry takes place (see Fig. 2). In general, the free energy depends on the vorticity $m=n_+-n_-$ and the total number of vortices in the system, $n=n_++n_-$. The transition at $(a/\xi)^2\sim 55$ and $\Phi/\Phi_0\sim 5.5$ takes place at the constant vorticity $m=3$ with the change of n from 5 to 3. The transition is therefore not only characterized by an order parameter, but also by the change of the number of vortices at the constant total vorticity m, suggesting that the transition is close to first order. This statement is confirmed by the observation that

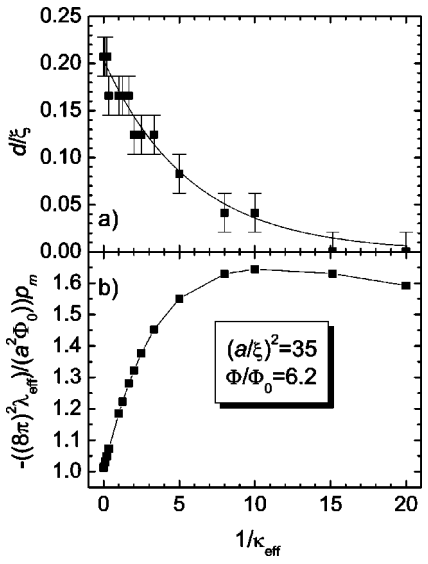

FIG. 5. The vortex-antivortex distance (a) and the magnetic moment of the sample (b) as functions of the parameter $1/\kappa_{eff}$. In (a) error bars represent the grid spacing and the solid line the exponential fit discussed in the text.

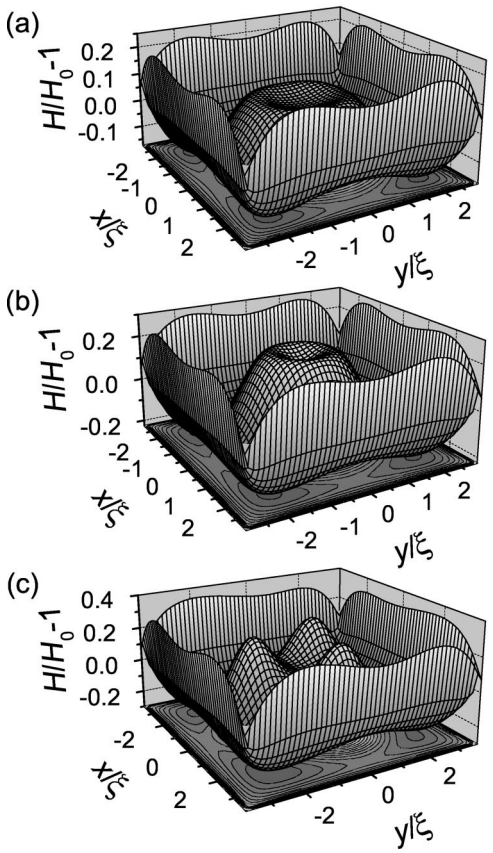

FIG. 6. The magnetic field in the film in the case of (a) giant vortex with $m=2$, (b) the antivortex solution with $m=4-1$, and (c) three separate vortices with $m=3$. Here H_0 is the external magnetic field.

above the transition point, $(a/\xi)>(a/\xi)_{crit}$, both solutions with $m=3$ and $m=4-1$ coexist (see Figs. 3 and 4). Since near the transition the free-energy difference between the phases with the same vorticity m and different n is small, it is difficult to determine the phase boundary between phases with $m=4-1$ and $m=3$ accurately. The transition could be easier observed by calculating the two-component order parameter $\eta_x=\int x|\psi(x,y)|^2dxdy$, $\eta_y=\int y|\psi(x,y)|^2dxdy$ shown in Fig. 3. The transition point is given by the point where the order parameter goes to 0. At the same point the calculated sample magnetization changes slope as is clearly seen from Fig. 4.

Close to the H_{c2} line the repulsion of vortices from the boundaries and attraction of the four vortices to the antivortex stabilize the phase with $m=4-1$ and small vortex-vortex distances. At smaller value of ξ the repulsion from the boundaries decreases and one vortex annihilates with the antivortex. As a result, the repulsion between the remaining vortices increases, leading to an increase of the order parameter with a further decrease of ξ.

Increasing the field up to $\Phi/\Phi_0=10.6$ leads to the stabilization of the phase with total vorticity $m=7$. Near the H_{c2} line similar to the phase with $m=4-1$ the solution with eight vortices and one antivortex $(m=8-1)$ is realized. When $(a/\xi)^2$ increases in a complete analogy to the case with $m=4-1$ the second-order phase transition to the phase

with seven vortices ($m=7$) and a similar order parameter takes place. Here, also, both solutions with $m=8-1$ and $m=7$ coexist above $(a/\xi)_{crit}$, indicating that the transition is close to first order. We believe that the situation is quite general for the case of arbitrary $m=4l-1$ for $l=1,2,3,\ldots$.

At the end we would like to discuss the dependence of the stability of the antivortex phase at small κ. According to the arguments of Ref. 6, at small κ the vortex-vortex interaction changes the sign, making the antivortex phase more stable. As a result, the average distance between vortices in the middle of the square increases as well. In order to verify this conjecture for the thin film sample we plot in Fig. 5 the vortex-antivortex distance r_0 as a function of $1/\kappa_{eff}$. The distance decreases with the decreasing κ_{eff}. For $\kappa_{eff}<0.1$ the distance is smaller than the grid spacing a/N, so we cannot resolve separate vortices. We find that $r_0 \propto \exp(-\Lambda/\lambda_{eff})$ with $\Lambda \sim a$. The situation is just opposite to that reported in Ref. 6. We believe that in the case of the thin film of square shape the reduction of κ does not stabilize the phase with the antivortex.

It is interesting to note differences between samples of different shapes. For the cylindric shape the giant-vortex phase with any vorticity is always stable close to the H_{c2} line.[7,8] According to the Ref. 6 for the mesoscopic triangle the giant-vortex state with $m=2$ is metastable and the solution with the antivortex ($m=3-1$) is stable. For the case of the square shape the giant-vortex solution with $m=3$ is *never* stable for $\kappa_{eff} \gtrsim 0.1$. For $\kappa_{eff}<0.1$ the limited grid spatial resolution prevented us from distinguishing the solution with the antivortex from the possibly (meta)stable giant-vortex solution.

Finally, let us discuss the possibility to detect the state with the antivortex experimentally. Calculation of the magnetic field in the sample shows that the magnetic field has a local minimum in the center of the sample also for the giant-vortex solution with $m=2$. The local minimum observed for the antivortex state with $m=4-1$ is therefore not due to the antivortex formation (Fig. 6) but due to a particular distribution of the current in the sample. Therefore, imaging of the magnetic field distribution cannot provide evidence for the antivortex. The magnetic field for the multivortex solution with $m=3$ has 3 well-separated maxima that break the fourfold rotational symmetry of the sample, allowing a direct imaging of vortices. Since the antivortex state cannot be detected directly, the observation of a hysteresis due to the antivortex metastability in the vicinity of the transition line from the $m=4-1$ antivortex state to the $m=3$ multivortex state could suggest that the symmetric phase is indeed the phase with the antivortex.

[1] L.F. Chibotaru, A. Ceulemans, V. Bruyndoncx, and V.V. Moshchalkov, Nature (London) **408**, 833 (2000).

[2] L.F. Chibotaru, A. Ceulemans, V. Bruyndoncx, and V.V. Moshchalkov, Phys. Rev. Lett. **86**, 1323 (2001).

[3] J. Bonca and V.V. Kabanov, Phys. Rev. B **65**, 012509 (2002).

[4] B.J. Baelus and F.M. Peeters, Phys. Rev. B **65**, 104515 (2002).

[5] A.S. Mel'nikov, I.M. Nefedov, D.A. Ryzhov, I.A. Shereshevskii, V.M. Vinokur, and P.P. Vysheslavtsev, Phys. Rev. B **65**, 140503 (2002).

[6] V.V. Moshchalkov (private communication); V.R. Misko, V.M. Fomin, J.T. Devreese, and V.V. Moschalkov, Phys. Rev. Lett. **90**, 147003 (2003).

[7] V.A. Schweigert, F.M. Peeters, and P.S. Deo, Phys. Rev. Lett. **81**, 2783 (1998).

[8] V.A. Schweigert and F.M. Peeters, Phys. Rev. Lett. **83**, 2409 (1999).